

The influence of strong tides on the formation of Amundsen Sea Polynya

Mengting Zhuo¹, Song Hu², Yu Hong³, and Yan Du⁴

¹State Key Laboratory of Tropical Oceanography, South China Sea Institute of Oceanology, Chinese Academy of Sciences; University of Chinese Academy of Sciences

²Shanghai Ocean University

³South China Sea Institute of Oceanology, Chinese Academy of Sciences

⁴State Key Laboratory of Tropical Oceanography, South China Sea Institute of Oceanology, Chinese Academy of Sciences; University of Chinese Academy of Sciences; Southern Marine Science and Engineerin

December 14, 2022

Abstract

Polynyas play an important role in climate change with an efficient exchange of heat and matter between the atmosphere and the ocean in polar regions. This study investigated the influence of strong tides and atmospheric forcing on the Amundsen Sea Polynya, especially focusing on large-area polynya events from 2002 to 2020. We found that the geographical locations of the polynyas are closely related to the underwater ridge, where tidal currents are relatively strong. More importantly, strong cross-ridge winds are the “triggers” above the sea surface for the initial formation of the Amundsen Sea Polynya, while strong tides under the sea surface tend to create large-area polynya. Four of the five largest polynya events occurred mainly during spring tides. Only the 2016 event occurred during the normal tide period, which was atmosphere-dominated. Strong tides significantly affect the evolution of polynyas by strengthening the vertical mixing of seawater. Given that ocean in Antarctica might become warmer, tidal mixing might enhance the mixing in the future climate.

Hosted file

951994_0_art_file_10528485_rms0h2.docx available at <https://authorea.com/users/566191/articles/612954-the-influence-of-strong-tides-on-the-formation-of-amundsen-sea-polynya>

The influence of strong tides on the formation of Amundsen Sea Polynya

Mengting Zhuo^{1,2}, Song Hu³, Yu Hong^{1,2}, and Yan Du^{1,2}

¹State Key Laboratory of Tropical Oceanography, South China Sea Institute of Oceanology, Chinese Academy of Sciences, Guangzhou, China.

²University of Chinese Academy of Sciences, Beijing, China.

³College of Marine Science, Shanghai Ocean University, Shanghai, China.

Corresponding author: Yan Du (duyan@scsio.ac.cn)

Key Points:

- The geographical location and shape of the Amundsen Sea Polynya were closely related to the underwater ridge (Bear Ridge).
- The atmosphere-dominated polynya event was caused by significant cross-ridge winds and surface net solar radiations.
- Four of the five largest polynya events occurred mainly during spring tides, which were tide-dominated events affected by the strengthening vertical mixing of seawater.

Abstract

Polynyas play an important role in climate change with an efficient exchange of heat and matter between the atmosphere and the ocean in polar regions. This study investigated the influence of strong tides and atmospheric forcing on the Amundsen Sea Polynya, especially focusing on large-area polynya events from 2002 to 2020. We found that the geographical locations of the polynyas are closely related to the underwater ridge, where tidal currents are relatively strong. More importantly, strong cross-ridge winds are the "triggers" above the sea surface for the initial formation of the Amundsen Sea Polynya, while strong tides under the sea surface tend to create large-area polynya. Four of the five largest polynya events occurred mainly during spring tides. Only the 2016 event occurred during the normal tide period, which was atmosphere-dominated. Strong tides significantly affect the evolution of polynyas by strengthening the vertical mixing of seawater. Given that ocean in Antarctica might become warmer, tidal mixing might enhance the mixing in the future climate.

Plain Language Summary

The polynya is a water area that does not freeze or has only thin ice when it reaches freezing conditions in winter. As a window between ocean and atmosphere, polynyas play an important role in climate change. The polynya is the result of the interaction of atmosphere, sea ice and ocean. This study focused on the major polynya events and the initial formation of the polynya using the sea ice concentration (SIC) data of the University of Bremen based on AMSR-E/2. We found that the geographical location of the polynya was closely related to the topography. The polynya extended to the open ocean along the terrain of the Bear Ridge. The formation of the Amundsen Sea Polynya was affected by the atmosphere and the ocean. Winds was the "triggers" for the formation of the Amundsen Sea Polynya. The wind field on the days when the Polynya splits was dominated by northwest and southeast winds (ESE, E, and WNW), which were cross-

40 ridge (Bear Ridge). The surface net solar radiations also played an important role in the area of
41 the Amundsen Sea Polynya. The area of the polynya was large during spring tides related to the
42 local spring tides, that is, the area was large during spring tides. Strong tides significantly affect
43 the evolution of polynyas by strengthening the vertical mixing of seawater. Ocean in Antarctica
44 might become warmer because of the global warming, tidal mixing may be more important for
45 the future climate.

46 **1 Introduction**

47 As one of Antarctica's fastest melting marginal seas, the Amundsen Sea is closely related to
48 the global climate and has become a hot area of geoscience (Kim et al., 2021). The Amundsen
49 Sea is located in West Antarctica (Figure 1), south of 71°S (100°W~135°W), on its east Thurston
50 Island, and its west Cape Dart, the cape of Siple Island, which is part of the South Pacific Ocean
51 connecting the Ross Sea and the Bellingsgauzen Sea. The Amundsen Sea is characterized by deep
52 troughs extending to the continental shelf fault (Jacobs et al., 2012). The direction of the extent
53 of the troughs is north-northeast, and the troughs gradually narrow towards the Pine Island
54 Trough with Bear Ridge on its west (Hogan et al., 2020).

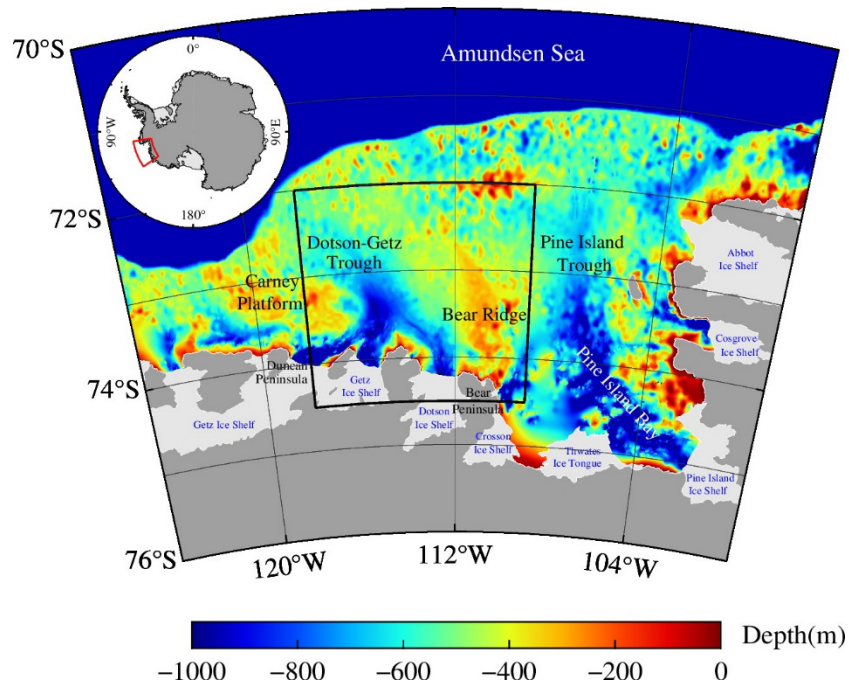
55 The melting of ice in the Amundsen Sea has been accelerating due to the rising global
56 temperatures (Nakayama et al., 2021). The mass loss rate of Antarctic glaciers gradually
57 increased from 40 ± 9 Gt/y in 1979-1990 to 252 ± 26 Gt/y in 2009-2017 (Rignot et al., 2019).
58 Among them, the loss of glacier mass in West Antarctica took place mainly in the Amundsen Sea
59 (Hogan et al., 2020; Rignot et al., 2019). Meanwhile, the mass loss rate of the Getz Ice Shelf in
60 the Amundsen Sea area was 16.5 Gt/y in 2017, three times higher than that in 1979-2003 (Rignot
61 et al., 2019). In addition, the Amundsen Sea played an important role in the mass balance of West
62 Antarctica glaciers and the rise in sea levels (Shepherd et al., 2019; Shepherd & Wingham,
63 2007). Thus, as the monitor of the Antarctic and global climate change, how the polynya in the
64 Amundsen Sea has changed in these years deserves our attention.

65 The Amundsen Sea Polynya is the main large polynya in Antarctica. A good number of
66 studies focused on its high primary productivity rather than its formation (Arrigo et al., 2012;
67 Lee et al., 2016; Thuróczy et al., 2012). A recent study by Macdonald et al. (Macdonald et al.,
68 2021) focused on the physical process of its formation. They found a concurrence of the highest
69 polynya areas in 2020 after April and the highest spikes in wind speed. However, as a window
70 connecting the atmosphere, sea ice, and ocean, the Amundsen Sea Polynya can be modified by
71 multiple factors.

72 Additionally, many studies have shown that polynyas are closely related to tides. In 1984 it
73 was proposed that tides play a major role in the polynya in the western Canadian Arctic (Melling
74 et al., 1984). Afterward, a study of the polynya in the Kashevarov Bank found in the Okhotsk
75 Sea showed that the resonance of the O_1 and K_1 harmonic constituents increased vertical heat
76 flux, which significantly affected the formation and change of the polynya (Martin, 2004). The
77 polynya showed an obvious two-week cycle in the winter of 2000-2001 (Martin, 2004). Tides
78 also impact the North Water Polynya, resulting in a 12-hour periodic change in the polynya
79 (Vincent & Marsden, 2008). The above studies mainly focused on the northern hemisphere
80 (Hannah et al., 2009). Possibly due to the remote location and great attention on the ice shelves,
81 so far as we know, there are yet no studies focusing on the impact of tides on the Amundsen Sea
82 Polynya. Previous studies have shown that tides can enhance the melting of the Amundsen Sea
83 ice shelves by increasing the exchange between ice and ocean (Jourdain et al., 2019). However,
84 the evolution of the Amundsen Sea Polynya related to tides attracts our attention after a detailed

85 examination.

86 Owing to the development of passive microwave remote sensing, AMSR-E data provided
 87 an opportunity to study the evolution of polynyas in much better detail than before. In this study,
 88 we used the sea ice concentration (SIC) data of the University of Bremen based on AMSR-E/2.
 89 We focused on the major polynya events and paid attention to the initial stages of the Polynya
 90 formation and the maximum area of each polynya. Furthermore, we comprehensively considered
 91 the oceanic factors (topography, tides) and atmospheric factors (wind, surface net solar radiation)
 92 of the Amundsen Sea, allowing us to analyze the mechanism of the large-area events from 2002
 93 to 2020.



94

95 **Figure 1.** The topography of the Amundsen Sea, Antarctica. The black line is the main area
 96 where polynyas occurred.

97 2 Data and methods

98 2.1 Data

99 The SRTM15+ V2.1 global bathymetry and topography dataset (Tozer et al., 2019) from
 100 Open Topograph (Wessel et al., 2019) was used for the bathymetry of the study region. The
 101 dataset used was the latest iteration of the SRTM+ digital elevation model (DEM) with a grid of
 102 15 arc seconds.

103 The sea ice concentration dataset, version 5.4 (Spren et al., 2008) from the University of
 104 Bremen, Institute of Environmental Physics (IUP) was used. The data was retrieved with the
 105 ARTIST Sea Ice (ASI) algorithm (Spren et al., 2008) based on AMSR-E (Advanced Microwave
 106 Scanning Radiometer for EOS, June 1st, 2002—October 4th, 2011) and AMSR2 (Advanced
 107 Microwave Scanning Radiometer 2, July 2nd, 2012—today). The data in HDF4 format with a
 108 spatial resolution of 3.125 km×3.125 km includes a daily time series of sea ice concentrations
 109 over the period 2002—2020 for the south polar regions, but the data from October 5th, 2011, to
 110 July 1st, 2012, and other individual times were missing.

111 Wind and surface net solar radiation data were all obtained from the European Centre for
 112 Medium-Range Weather Forecasts (ECMWF) ERA5 dataset. The dataset was obtained from the
 113 Copernicus Climate Change Service (C3S) at ECMWF. We combined the eastward and
 114 northward components of the 10m wind to give the speed and direction of the horizontal 10m
 115 wind. These data with a spatial resolution of $0.25^{\circ} \times 0.25^{\circ}$ have a temporal resolution of 1 day. If
 116 the vertical heat flux (surface net solar radiation) is positive, the heat transfer direction is
 117 downward.

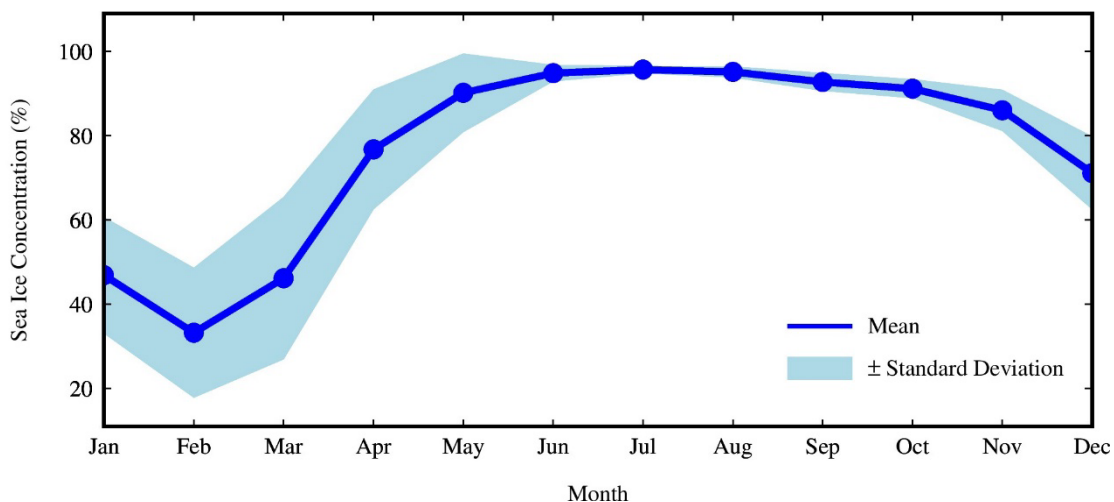
118 TPXO tide models (Egbert & Erofeeva, 2002) developed by the Oregon State University
 119 (OSU) were used to predict the tide level. TPXO9-atlas models have a spatial resolution of $1/30^{\circ}$
 120 globally provided by National Computational Infrastructure (NCI). The models include 8
 121 primary (O_1 , K_1 , S_2 , P_1 , M_2 , N_2 , Q_1 , and K_2) and 4 non-linear ($2N_2$, M_4 , MS_4 , and MN_4) harmonic
 122 constituents. A position of $112^{\circ}W$ and $73^{\circ}S$ was chosen to represent the study region, and a tide
 123 level from 2002 to 2020 was obtained.

124 2.2 Methods

125 2.2.1 Study time

126 The timing of freezing and melting of sea ice in the Amundsen Sea differs from that in other
 127 regions of Antarctica, which have certain regional characteristics (Stammerjohn et al., 2012). The
 128 monthly sea ice concentration in the Amundsen Sea ($125^{\circ}W \sim 99^{\circ}W$, $76^{\circ}S \sim 70^{\circ}S$) from 2002 to 2020
 129 was 33.29%-95.73% (Figure 2). On average, sea ice concentration was lowest in February and
 130 highest in July. Interannual sea ice variation was greatest in March, the early stages of glaciation,
 131 with a standard deviation of 19.22%. Sea ice concentration was relatively stable in July, which
 132 was the highest value of sea ice concentration in those years, with a standard deviation of 0.84%.
 133 Because the polynya is an area that is not covered by sea ice when it reaches the freezing
 134 condition. June to October was selected as the study period for polynyas, with high sea ice
 135 concentration and low interannual sea ice variation.

136

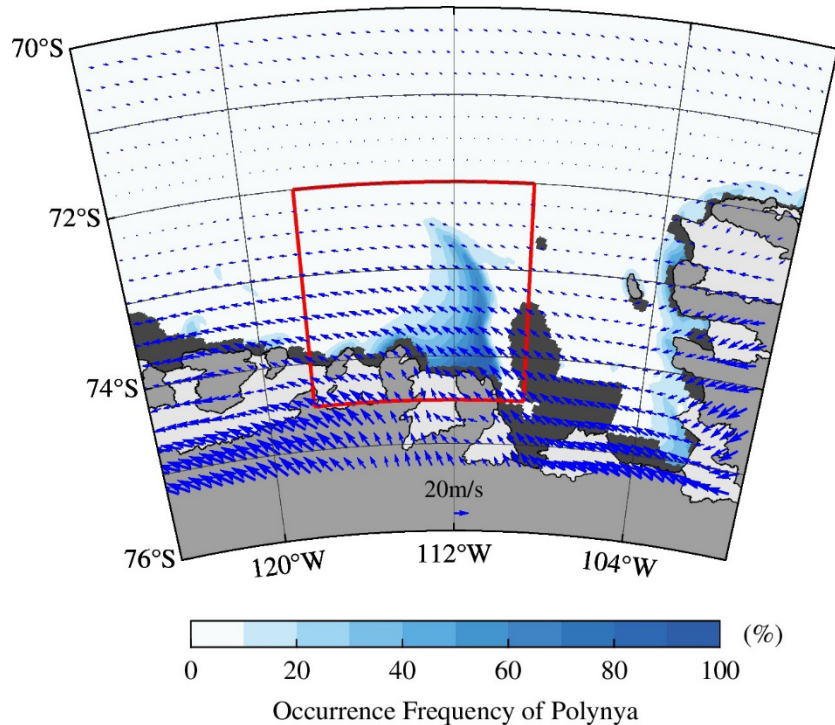


137

138 **Figure 2.** The monthly sea ice concentration in the Amundsen Sea (125°W~99°W, 76°S~70°S)
 139 from 2002 to 2020. The blue line is the mean sea ice concentration of each month, and the
 140 shaded blue is the standard deviation of the mean sea ice concentration for each month in 19
 141 years.

142 2.2.2 Study site

143 Polynyas can generally be distinguished by sea ice concentration and sea ice thickness
 144 (Massom et al., 1998; Preusser et al., 2019). In this study, polynyas are distinguished by the sea
 145 ice concentration, and the 75% sea ice concentration value is taken as the threshold for judging
 146 the polynya (Massom et al., 1998). It is considered that the area with less than 75% sea ice
 147 concentration is the polynya area, and the area with more than 75% sea ice concentration is the
 148 sea ice area. Thus, the occurrence frequency of the Polynya in the Amundsen Sea from 2002 to
 149 2020 was evaluated (Zhang et al., 2021). The main area of polynya in the Amundsen Sea was
 150 assumed to be the area with a high occurrence frequency (Figure 3). The Amundsen Sea is
 151 normally covered by sea ice from June to October. However, along the Bear Ridge and the east
 152 coast of Pine Island Bay, one large polynya and a series of coastal polynyas always regularly
 153 occurred during this period. Therefore, waters of Amundsen Sea Polynya (118W~109W,
 154 74.5S~72S) with high occurrence frequency were framed with solid red lines, which was
 155 selected as the main study area (Figure 3). The Amundsen Sea Polynya is a perennial water area
 156 surrounded by high sea ice. Most of the time, the shape of polynya was an arc, extending
 157 northward from the coast of Bear Ridge with the tip facing west.
 158



159

160 **Figure 3.** The occurrence frequency of polynya and mean wind field distribution in the
 161 Amundsen Sea over the period 2002-2020. The solid red lines is the main study area.

162 2.2.3 Calculation of polynya area

163 The sea ice concentration data with a spatial resolution of 3.125 km×3.125 km was used in
 164 this study. According to each grid area, the area of the Amundsen Sea Polynya was calculated by
 165 water area integral:

$$166 S = \int (1 - C) ds \quad (1)$$

167 Where C is the sea ice concentration, s is the single grid area (with 75% sea ice
 168 concentration value as the threshold), and S is the area of the polynya.

169 3 Results

170 3.1 Impact of cross-ridge wind on triggering polynya

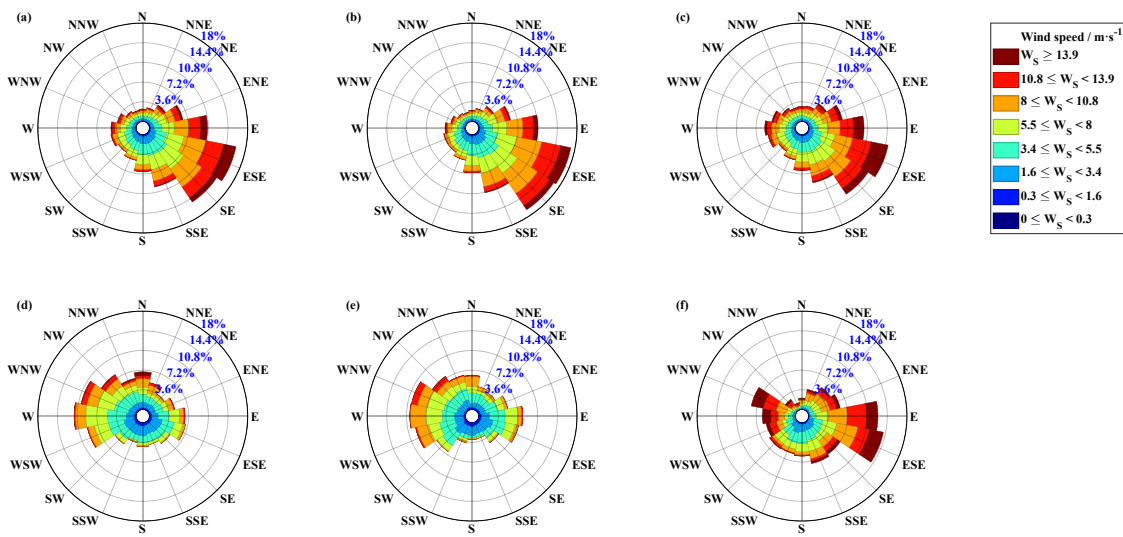
171 The mean wind speed in the Amundsen Sea area (125°W~99°W, 76°S~70°S) from June to
 172 October 2002 to 2020 was 8.05 m/s. As seen in Figure 3, the mean wind field had a good
 173 relationship with the occurrence frequency of Amundsen Sea Polynya. The wind speed along the
 174 coast of the study area (red frame) was large, and the overall wind direction was offshore, south-
 175 easterly. It was a cross-ridge wind that roughly coincided with the splitting direction of the
 176 Polynya and was perpendicular to the direction of the Polynya extension.

177 The area of the Polynya is generally 10-10⁵ km² (Morales Maqueda et al., 2004), and the
 178 mean area of the Amundsen Sea Polynya in winter was 4.53 × 10³ km². Results showed that
 179 when the area of the Amundsen Sea Polynya was less than 400 km², this identified a situation of
 180 complete ice cover in the study area. If the area of the Amundsen Sea Polynya exceeds 400 km²
 181 one day and this day is the day after a completely freezing day, this day is the day when the
 182 Polynya splits and the first day of a polynya event. The period from this day to the next complete
 183 ice cover is considered as a complete Amundsen Sea Polynya event. For example, in 2018, the
 184 study area was completely covered by sea ice from August 2nd to 4th and September 22nd, the area
 185 of the Polynya exceeded 400 km² from August 5th to 21st. It was considered that the period from
 186 August 5th to September 22nd was a complete Amundsen Sea Polynya event. It was considered
 187 that August 4th is the day before the Polynya splits, and August 5th is the day when the Polynya
 188 splits. The Amundsen Sea Polynya happened in most cases from June to October every year, and
 189 was completely covered by sea ice for only 163 days in 19 years.

190 Studies have shown that some large polynya events may be caused by strong wind events
 191 (Macdonald et al., 2021). The change of the Amundsen Sea Polynya affected by the wind field
 192 occurred mainly on the synoptic scale in terms of time. Using the Beaufort scale (Penwarden,
 193 1973), the wind field in the study area was dominated by southeast offshore winds all year round
 194 (Figure 4a). ESE was the main wind direction, accounting for 16.19 %. In contrast, the
 195 proportion of westerly wind direction was relatively low. Figures 4b and 4c show the distribution
 196 of the mean wind speed and direction in the study area from January to May in summer and June
 197 to October in winter, respectively. The relative proportion of each wind direction in summer and
 198 winter was consistent with the distribution of wind direction throughout the year, mainly
 199 dominated by southeast winds (ESE and SE). The proportion of higher wind speeds in winter
 200 was higher than in summer. The proportion of higher wind forces of 7 and above (>13.9 m/s)
 201 was only 4.86 % in summer, while it accounted for 9.74 % in winter.

202 On days with complete frost, before and after the formation of the Polynya, the wind field

203 distribution in the study area was very different from that in normal times (Figure 4d-f). On days
 204 with complete frost and the days before the Polynya split (Figure 4d, e), the main wind direction
 205 was Northwest (W and WNW). However, the main wind directions, which were Southeast (ESE
 206 and E) and Northwest (W and WNW) in the study area, were cross-ridge on the days when the
 207 Polynya splits (Figure 4f). The proportion distribution of the individual wind directions was
 208 completely different from when it was frozen and the days before the Polynya splits. Compared
 209 to the long-term mean wind field, the westerly wind direction (WNW and W) had a large
 210 proportion on the day when the Polynya splits, followed by the largest proportions of the ESE
 211 and E directions with about 8.26% and 6.07%, respectively. In particular, on the day when the
 212 Polynya splits, the wind speed was great. The proportion of higher wind speeds of force 7 and
 213 above was high at 13.09%. The wind direction was generally dominated by the northwest coastal
 214 winds when it was fully frozen and the days before the Polynya splits. Therefore, the northwest
 215 coastal winds were conducive to the Polynya area being completely covered by sea ice. The
 216 strong cross-ridge wind in the study area could easily blow away the sea ice, leading to the
 217 formation of the Polynya.
 218



219

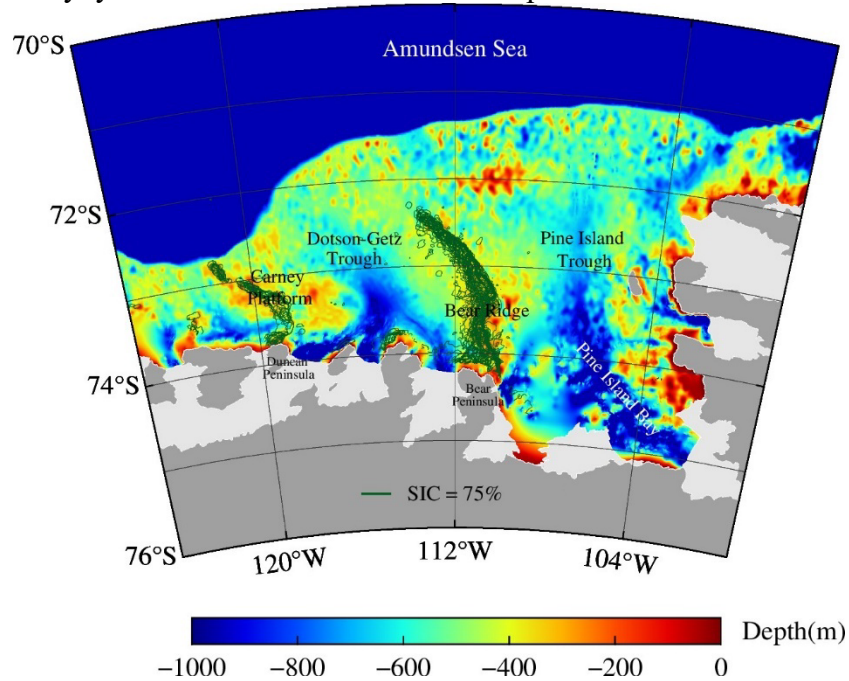
220 **Figure 4.** The percentage distributions of wind speed and direction in different times **a.** all days,
 221 **b.** the days from January to May in summer, **c.** the days from June to October in winter, **d.** the
 222 completely freezing days, **e.** the days before the Polynya splits and **f.** the days when the Polynya
 223 splits over the period 2002-2020. Solid red lines is the main study area.

224 3.2 Impacts of the ridge on the Polynya

225 The continental shelf narrows from east to west and the depth north of it exceeds 1000 m
 226 (Figure 5). Along the coast, there are two deep inland shelf troughs with the longitude of about
 227 115°W and 106°W and a depth of more than 1000 m. There are two areas with shallow depth to
 228 the west and in the middle of the two troughs. The Carney platform near 119°W to the west has
 229 relatively high terrain and a depth of about 100 m to 200 m. The Bear Ridge 111°W to the east is
 230 also relatively shallow and extends west toward the open ocean.

231 When the area of the Amundsen Sea Polynya was small, regardless of the small water area

232 to the north of 72°S, we could observe that the Polynya matched perfectly with the bathymetry,
 233 mainly distributed in an arc from the coast to the outside. Figure 5 shows the situation of all the
 234 days during the initial period of the Polynya splitting, when the Polynya was small in the
 235 Amundsen Sea from June to October 2020. The Polynya started from the Bear Peninsula near
 236 111°W, extended to the open ocean in the north along the topography of the Bear Ridge, and the
 237 northernmost tip of it faced west. Furthermore, there was also an occasional polynya in the
 238 Amundsen Sea in 2020, extending along the topography from the Duncan Peninsula near 119°W
 239 to the edge of the western continental shelf along the Carney Platform. The shape of the Polynya
 240 was also similar to that of the Amundsen Sea Polynya. They were both shaped as an arc, with the
 241 northernmost tip facing west. It could be seen that the topography plays an important role in the
 242 formation of the Polynya and affects its location and shape.



243
 244 **Figure 5.** The topography and the distribution of the Polynya (green lines) during the initial
 245 splitting period of the Amundsen Sea Polynya from June to October 2020.

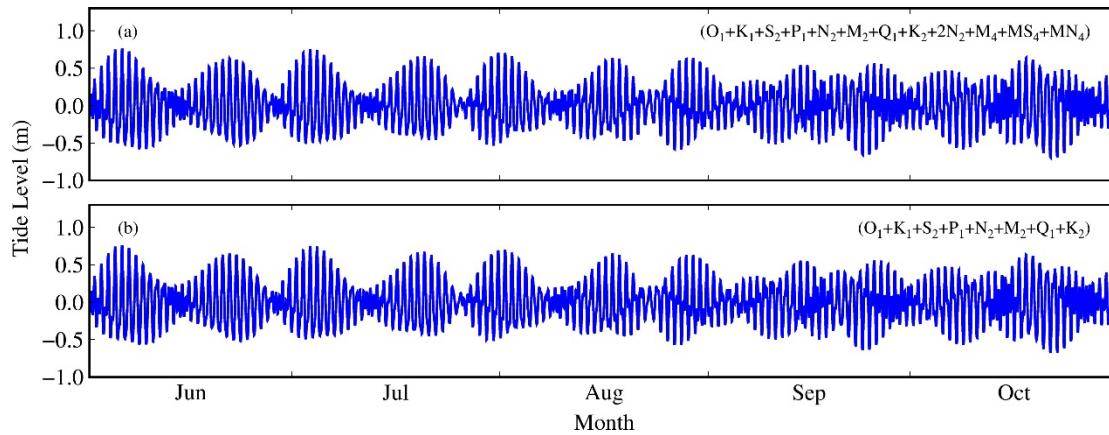
246 3.3 Large-area polynya events

247 3.3.1 Tides

248 **Figure 1.** Amplitude and phase lag of harmonic constituents.

harmonic constituent	amplitude/ m	phase lag/ $^{\circ}$	harmonic constituent	amplitude/ m	phase lag/ $^{\circ}$
O ₁	0.244	99.9	Q ₁	0.054	89.7
K ₁	0.174	87.1	K ₂	0.033	163
S ₂	0.134	160.7	2N ₂	0.011	176
P ₁	0.107	118.4	M ₄	0.003	83.2
M ₂	0.063	-107.5	MS ₄	0	166.8
N ₂	0.061	-160	MN ₄	0	39.6

249
250
251



252

253 **Figure 6.** The time series of tide level in the study site from June to October in 2020. **a.**
254 including 8 primary (O_1 , K_1 , S_2 , P_1 , M_2 , N_2 , Q_1 and K_2) and 4 non-linear ($2N_2$, M_4 , MS_4 and
255 MN_4) harmonic constituents, **b.** only including 8 primary harmonic constituents.

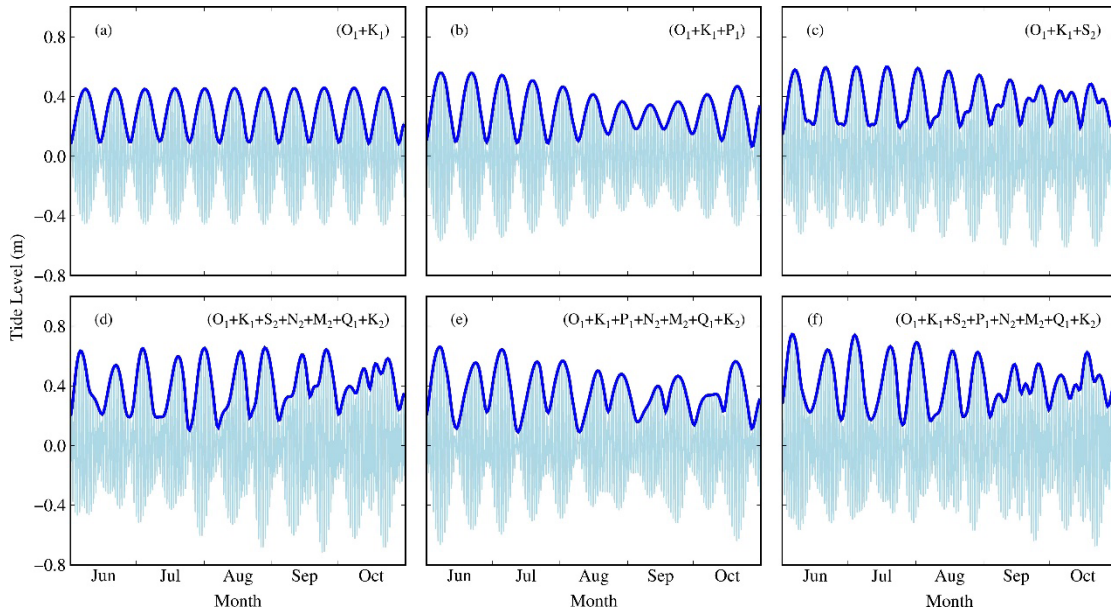
256

257 The position (112°W , 73°S) was chosen to investigate the tides in the study region. Taking
258 the tide level from June to October in 2020 as an example, the amplitude of O_1 , K_1 , S_2 , P_1
259 primary harmonic constituents were higher (above 0.1m) than in other months. There were four
260 extremely low non-linear ($2N_2$, M_4 , MS_4 , and MN_4) harmonic constituents, and we ignored them
261 by comparing Figure 6a and Figure 6b. There were two high and two low water in this site in a
262 day, which belongs to the irregular semidiurnal tide. The tides from June to August in the
263 Amundsen Sea area generally alternated between a 16-day cycle and a 12-day cycle. Based on
264 the spring tide from June to August, there were still some spring tides with relatively low tide
265 levels in September and October. The frequency of spring tides in these two months was
266 relatively high.

267 We presented the tides, including 2 primary (O_1 and K_1) harmonic constituents in Figure 7a.
268 In Figure 7b, we considered P_1 primary harmonic constituents based on Figure 7a. By comparing
269 them, it could be considered that spring tides changed because of P_1 . Unlike Figure 7a, there
270 were regular tides in Figure 7a with a tide level of 0.43m at high water hours. The tide level of
271 spring tides changed. Thus, the tide level of spring tides reached the lowest value in early
272 September, at 0.33m. We presented the tides, including all primary harmonic constituents (O_1 ,
273 K_1 , S_2 , P_1 , M_2 , N_2 , Q_1 , and K_2) in Figure 7f, but did not consider P_1 primary harmonic
274 constituents in Figure 7d. We can also draw the conclusion that P_1 played an important role in
275 lowering the tide level of spring tides but raising the tide level of neap tides in early September.

276 Similarly, we considered the role of S_2 in the site by comparing Figure 7a with Figure 7c
277 and comparing Figure 7e with Figure 7f. It was observed that S_2 made spring tides higher, which
278 was most obvious in July. It also increased the original neap tides and became part of some low
279 spring tides. There were two similar level spring tides in October because of S_2 , so the spring
280 tides' frequency increased. Thus, by detailed examination, we considered that P_1 and S_2 were two
281 of the most important harmonic constituents contributing to the irregular pattern of tides in the
282 region.

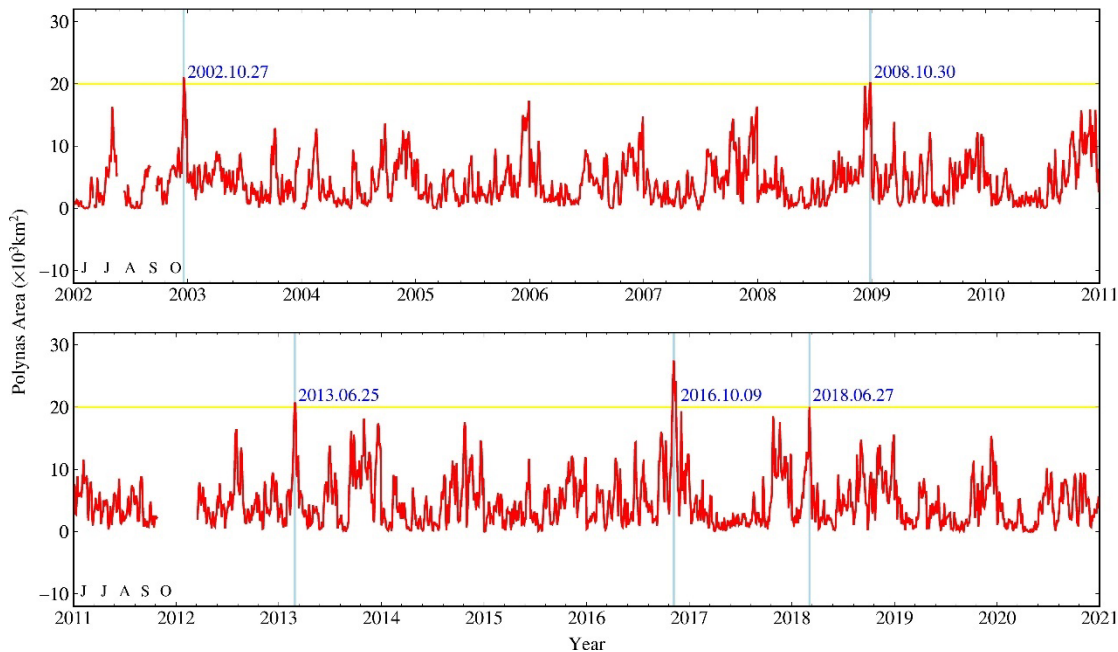
283



284

285 **Figure 7.** Tide level was most significantly affected by P_1 and S_2 primary harmonic constituents
 286 in the study site from June to October 2020. In this part, only the 8 primary harmonic
 287 constituents were considered. **a.** the tides including 2 primaries (O_1 and K_1) harmonic
 288 constituents, **b.** on the basis of **a.**, consider P_1 primary harmonic constituents, **c.** on the basis of
 289 **a.**, consider S_2 primary harmonic constituents, **f.** including all primary (O_1 , K_1 , S_2 , P_1 , M_2 , N_2 , Q_1
 290 and K_2) harmonic constituents, **d.** on the basis of **f.**, did not consider P_1 primary harmonic
 291 constituents, **e.** on the basis of **f.**, did not consider S_2 primary harmonic constituents.

292 3.3.2 Impacts of tides on polynya



293

294 **Figure 8.** The time series of the Polynya area from June to October over the period 2002-2020.
 295 The yellow line indicates the value of $20 \times 10^3 \text{km}^2$ to find the five largest-area polynya events.
 296 The dates of the five largest-area events are marked with blue lines.

297
 298 According to the time series of the Amundsen Sea Polynya area (Figure 8), five large-area
 299 polynya events with an area of more than $20 \times 10^3 \text{km}^2$ were selected to analyze the
 300 environmental characteristics before their occurrence. The study area was represented by the
 301 position (112°W , 73°S), and the TPXO9-atlas models, including 8 primaries (O_1 , K_1 , S_2 , P_1 , M_2 ,
 302 N_2 , Q_1 , and K_2) and 4 non-linear ($2N_2$, M_4 , MS_4 , and MN_4) harmonic constituents were used for
 303 tide prediction. It could be seen from the prediction that the tide in the study area belonged to an
 304 irregular semidiurnal tide. We found that four of the five events (events B-F) with the largest area
 305 of the Polynya occurred within 3 days after the spring tide (Table 2), which may be a tide-
 306 dominated polynya. Therefore, it suggested that the tides may be a factor in the change of the
 307 Amundsen Sea Polynya. Unlike regular tides patterns in similar studies on the northern
 308 hemisphere (Hannah et al., 2009; Martin, 2004; Melling et al., 1984; Vincent & Marsden, 2008),
 309 the irregular tides pattern caused by P_1 and S_2 makes the study on the link between tides and
 310 polynyas more complex.

311

312

Figure 2. Analysis of the characteristics of large polynya events.

Events	Maximum area ($\times 10^3 \text{km}^2$)	Maximum area occurrence time	Time of last spring tide	Days from spring tide	Mean surface net solar radiation in the first five days ($\times 10^5 \text{J} \cdot \text{m}^{-2}$)
A	27.50	2016.10.09	2016.10.04	5	1.39
B	21.08	2002.10.27	2002.10.24	3	2.95
C	20.74	2013.06.25	2013.06.22	3	0
D	20.29	2008.10.30	2008.10.30	0	3.41
E	20.04	2018.06.27	2018.06.26	1	0

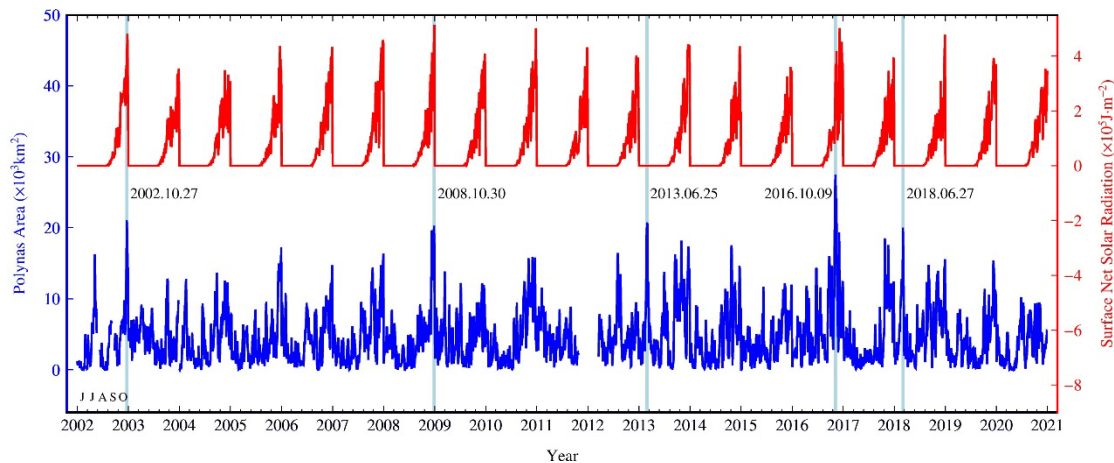
313

314 It can be seen from Table 2 that the mean surface net solar radiation five days before the
 315 Polynya events was very different. This was because they occurred in different months, in June
 316 and October, respectively. The surface net solar radiation in June was $0 \text{J} \cdot \text{m}^{-2}$ (Figure 8), and
 317 the radiation in October was large. The radiation in the first five days of events A, B and D in
 318 October exceeded the mean surface net solar radiation in the study area (Table 2). Event A was
 319 the largest polynya event in 19 years. In this event, the date when the area of the Polynya
 320 exceeded $20 \times 10^3 \text{km}^2$ was October 7th-12nd. Although the largest area of this event did not occur
 321 during the spring tide, the area also exceeded $20 \times 10^3 \text{km}^2$ on the third day after spring tide,
 322 which provided a basis for the occurrence of the largest area. Moreover, the mean radiation in the
 323 first five days was large, and it was characterized by the strong cross-ridge wind from October
 324 2nd to October 9th. This event did not disappear until October 17th. Therefore, we consider that
 325 this event was an atmosphere-dominated event, which was caused by unusually significant cross-
 326 ridge wind and surface net solar radiation.

327 3.4 Impact of surface net solar radiation on polynya

328 The net surface solar radiation in the study area from June 1st to August 23rd throughout the

329 19 years was $0 J \cdot m^{-2}$ (Figure 9). Radiation gradually increased from the end of August every
 330 year; In addition, radiation peaked in winter at the end of October. The mean net insolation at the
 331 surface from September to October 2002 to 2020 in the study area was $1.37 \times 10^5 J \cdot m^{-2}$.
 332 Compared to the time series of the Amundsen Sea Polynya, it can be seen that late October, with
 333 large surface net insolation, was generally the time when the area of the Polynya was the largest.
 334 The Polynya area was also large in the three years of large-scale net solar radiation in 19 years
 335 (2002, 2008, and 2017). It is worth noting that on October 31st, 2008, net solar radiation at the
 336 surface reached its highest level making it the fourth largest polynya in 19 years with a total area
 337 of $5.14 \times 10^5 J \cdot m^{-2}$. In addition, on October 9th, 2016, the area of the Polynya reached $2.75 \times$
 338 $10^4 km^2$, the maximum in 19 years. The surface net solar radiation in October of this year was the
 339 second largest value in 19 years, only after 2008. There is an apparent corresponding relationship
 340 between the surface net solar radiation and the area of the Polynya. The area with large surface
 341 net solar radiation in the ocean hinders the generation of sea ice, which is conducive to the
 342 formation and development of polynya. When the polynya is large, it can absorb more solar
 343 radiation due to the lack of sea ice coverage with higher albedo. The surface net solar radiation
 344 of the ocean is thus increased, which may make the polynya have a larger area. Therefore,
 345 because of the positive feedback relationship between sea ice and solar radiation, the surface net
 346 solar radiation is of great significance for the polynya.
 347



348

349 **Figure 9.** The time series of the Polynya area and the surface net solar radiation from June to
 350 October 2002-2020. The blue line indicates the Polynya area and the red line is the surface net
 351 solar radiation in 19 years (the positive values in the radiation indicate that the heat transfer
 352 direction is downward).

353 4 Discussion

354 4.1 Impacts of oceanic factors on polynya

355 As a key channel for the interaction between the atmosphere, ice, and ocean, the Amundsen
 356 Sea Polynya offers a unique perspective on climate change. With the development of field
 357 observation and marine satellite remote sensing, more and more ocean data are available for
 358 studying polynya. The remote Amundsen Sea has also received increased attention (Jacobs et al.,
 359 2012) and topographical data in the vicinity of the Amundsen Sea has been continuously updated
 360 (Hogan et al., 2020; Nitsche et al., 2007), laying the foundations for an oceanographic

361 exploration of the Amundsen Sea. It was found that Amundsen Sea Polynya existed in most cases
362 from June to October every year, but was completely frozen for only 163 days in 19 years. The
363 mean area of the Amundsen Sea Polynya was $4.53 \times 10^3 \text{ km}^2$ in winter, reaching the maximum
364 area of $2.75 \times 10^4 \text{ km}^2$ on October 9th, 2016. In general, the area of the Polynya reached a large
365 value at the end of winter (October). Arrigo et al. (Arrigo et al., 2012) showed that the mean area
366 of the Amundsen Sea Polynya was about $2.7 \times 10^4 \text{ km}^2$ in spring and summer, and the area
367 decreased to less than 10000 km^2 by the end of March. This was different from the calculation in
368 this study, which may be due to the different selection of study area and study period.

369 Ocean changes play an important role in sea ice and polynya in the Antarctic (Hellmer et al.,
370 2012) and can affect the stability of the ice shelves in the West Antarctic (Jacobs et al., 2012). It
371 was an important pillar in maintaining the existence of polynya (Parkinson, 1983). Previous
372 studies have shown that the distribution of the Weddell Sea Polynya and its nearby vertical heat
373 flux was affected by topography (Maud Rise) (Bagriantsev et al., 1989; Gordon & Huber, 1990).
374 And there have been models explaining the reasons for the formation and maintenance of the
375 Weddell Sea Polynya, which could be due to the increase in seawater mixing due to topography
376 (Ou, 1991). Similarly, the Amundsen Sea Polynya matched well with the topography (the Bear
377 Ridge) in the initial stage of the formation of the Amundsen Sea Polynya, which was mainly
378 distributed in an arc from the coast to the open ocean.

379 As a periodic ocean phenomenon, tides also significantly affect the changes in regional
380 polynyas. Compared to the northern hemisphere, the Antarctic is more difficult to access. We
381 found that the Amundsen Sea tides are influenced by the harmonic constituents S_2 and P_1 .
382 Although the mean cycle of the spring tide was 14 days, it was very erratic, making the
383 corresponding comparison between spring tide and polynya not so straightforward. Unlike
384 others, the change in polynyas due to the action of tides had a relatively clear cycle (Martin,
385 2004; Vincent & Marsden, 2008). However, it is worth noting that there were four major polynya
386 events at the Amundsen Sea, all of which occurred within 3 days of the spring tide. The tides
387 may play some role in the formation of the Amundsen Sea Polynya. In addition, larger waves
388 during spring tide may also be one of the reasons for polynya areas, which need to be further
389 studied.

390 Similar to recent studies on ice shelf melting, they found that tides are closely related to the
391 melting of Antarctic ice shelves (Hausmann et al., 2020; Huot et al., 2021; Jourdain et al., 2019;
392 Richter et al., 2022). Tides increase the vertical mixing of seawater, so the kinetic energy of the
393 current increases in contact with ice shelves (Hausmann et al., 2020). Tides thus contribute
394 greatly to the exchange of heat and salt between the ice and the ocean (Richter et al., 2022).
395 Tides have been shown to enhance ice shelf melting in the Amundsen Sea by increasing heat flux
396 transfer between sea ice and the ocean (Jourdain et al., 2019; Richter et al., 2022). Similarly, in
397 the D'Urville Sea, it has been found that at low tide, ice shelf ground melt increases (Huot et al.,
398 2021). But we do not currently know the specific effect of the tides on the polynyas. In the
399 follow-up work, it is necessary to strengthen the study of the relationship between local tides and
400 polynyas. It is particularly important to make clear the mechanism of tides on the Amundsen Sea
401 Polynya.

402 4.2 Impacts of atmospheric factors on polynya

403 Atmospheric action is also very important for polynya formation, and the wind is the key
404 factor for polynya formation (Parkinson, 1983). Coastal polynya is the result of sea ice advection
405 caused by wind. The size of the polynya depends on the duration and intensity of the wind

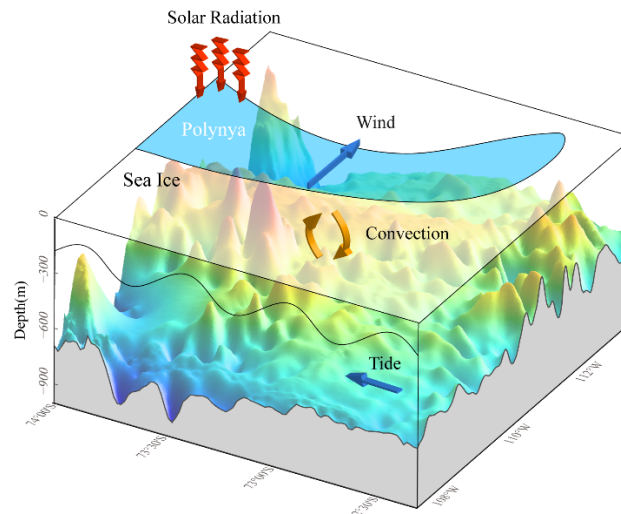
406 (Comiso et al., 2011). There was a good correspondence between the mean wind field in the
407 study area and the occurrence frequency of the Amundsen Sea Polynya. This was consistent with
408 the results of MacDonald et al. (Macdonald et al., 2021) on the spatial distribution of the mean
409 wind field in the Amundsen Sea. And they found that the daily mean wind speed had a weak
410 positive correlation with the area of the Polynya in the Amundsen Sea. Furthermore, showing the
411 wind field with wind roses, we add that the Amundsen Sea Polynya was directly related to the
412 cross-ridge wind in the site. The wind speed along the coast was large, and the direction was
413 cross-ridge, which was roughly consistent with the splitting direction of the Polynya and
414 perpendicular to the Amundsen Sea Polynya extent. Similarly, studies near the Halley research
415 station also showed that the formation and closure of polynyas were highly related to winds
416 (Markus & Burns, 1993). The change of the Amundsen Sea Polynya affected by the wind field is
417 mainly the synoptic scale in terms of time (Arrigo et al., 2012). Before and after the formation of
418 the Polynya, the wind field distribution in the study area was very different from that in normal
419 times. On the day when the Polynya splits, the main wind direction in the study area was
420 southeast (ESE and E) and northwest (W and WNW). The northwest and southeast winds were
421 cross-ridge, perpendicular to the terrain of Bear Ridge, which easily blew away the sea ice,
422 resulting in the formation of the Polynya.

423 Solar radiation enters the ocean surface, melting the sea ice and leading to the generation of
424 polynyas (Morales Maqueda et al., 2004). There was an obvious relationship between the surface
425 net solar radiation and the area of the Polynya. The area of the Polynya during 19 years was
426 greater for three years (2002, 2008 and 2017) associated with large surface net solar radiations.
427 The area of the Polynya reached its maximum value on October 9th, 2016. The surface net solar
428 radiation in October of that year was the second largest value in 19 years. Tides were not the
429 cause of the largest polynya events on October 9th, 2016. The area of the Polynya will increase
430 with the increase of the surface net solar radiation, due to the positive feedback relationship
431 between the polynya and the surface net solar radiation. We considered that this event was an
432 atmosphere-dominated event, which was caused by a large surface net solar radiation and a
433 special air-sea interaction condition.

434 The Amundsen Sea Polynya reached the maximum area on October 9th, 2016. This year has
435 been greatly studied and could be a special year that could be affected by the significant strong
436 El Niño phenomenon in 2015-2016 (Meehl et al., 2019). From September to October 2016, the
437 Antarctic experienced a sharp decline in sea ice cover (Meehl et al., 2019). The sea ice melting
438 time unusually advanced in 2016. The time when the sea ice range in Antarctica reached its
439 maximum advanced from September to August (Schlosser et al., 2018). MacDonald et al.
440 (Macdonald et al., 2021) also showed that there were records of low sea ice conditions from
441 2016 to 2017, which significantly affected the Amundsen Sea Polynya area. Thus, we think that
442 the effect of the atmosphere was more significant than that of tides in this special year, so one of
443 the large polynya events did not occur during spring tides. However, the remaining four large
444 polynya events occurred during spring tides, suggesting that tides were more common factors.

445 Many studies have shown that the sea water in the west Antarctic is warming (Spence et al.,
446 2017). Tides can more effectively transfer heat to polynyas through mixing. Meanwhile, studies
447 have shown that the sea ice in Antarctica is facing great changes (Thompson, 2022). These all
448 mean that tides will play an increasingly important role in the study of polynyas in the future.

449 **5 Conclusions**



451

452 **Figure 10.** Schematic diagram of the formation and development of the Amundsen Sea Polynya.

453

454 This study focused on the polynya events and the change in the area of the Amundsen Sea
 455 Polynya from 2002 to 2020. According to the results, we summarized the influence of oceanic
 456 and atmospheric factors on the formation and development of the Amundsen Sea Polynya
 457 (Figure 10). The geographical location and shape of the Amundsen Sea Polynya were closely
 458 related to the topography, mostly in crescent. The Amundsen Sea Polynya began on Bear
 459 Peninsula and extended along the terrain of Bear Ridge to the open ocean. The "trigger" of the
 460 Amundsen Sea Polynya events is wind, which is the key factor in the formation of the polynya.
 461 The formation of the polynya is related to the synoptic scale wind field. The characteristics of the
 462 wind field before and after the formation of the polynya were very different. The wind during the
 463 formation of the polynya was mainly cross-ridge and observed to be perpendicular to the terrain
 464 of Bear Ridge in the Southeast (ESE and E) and Northwest (W and WNW).

465 Further more, this study found that the tides play a significant role in the formation of the
 466 polynyas. The present study shows that four of the five extreme events with the largest area of
 467 the Polynya may be tide-dominated. The fifth extreme event was atmosphere-dominated, caused
 468 by significant cross-ridge winds and surface net solar radiations. This shows that tides can
 469 generally provide favorable conditions for the development of the polynya, particularly for large-
 470 scale events, which has not been accounted for in most studies for polynya in Antarctica. Due to
 471 the effect of tides, the vertical convection and mixing of seawater are strengthened. The warmer
 472 seawater in the interior of the ocean is conducive to the formation and development of polynyas.
 473 Tides was the main energy source for the enhanced dissipation along the continental slopes,
 474 which was correlated with the tidal energy dissipation rate (Rippeth et al., 2015). Rough
 475 topography can influence the mixing of seawater. In addition, the interaction between tides and
 476 rough topography affects the rate of mixing. With the impact of global warming, the increase of
 477 heat transport from the atmosphere to the ocean, the decrease of sea ice, and the enhancement of
 478 mixing caused by tides need more attention.

479 Acknowledgments

480 This work is supported by the National Natural Science Foundation of China (41830538),
 481 National Key R&D Program of China (2018YFA0605704), and the Chinese Academy of

482 Sciences (133244KYSB20190031, 183311KYSB20200015, and SCSIO202201).

483 **References**

484 Arrigo, K. R., Lowry, K. E., & van Dijken, G. L. (2012). Annual changes in sea ice and
485 phytoplankton in polynyas of the Amundsen Sea, Antarctica. *Deep Sea Research Part II:
486 Topical Studies in Oceanography*, 71-76, 5-15. <http://doi.org/10.1016/j.dsr2.2012.03.006>

487 Bagriantsev, N. V., Gordon, A. L., & Huber, B. A. (1989). Weddell Gyre: Temperature
488 maximum stratum. *Journal of Geophysical Research*, 94(C6), 8331.
489 <http://doi.org/10.1029/JC094iC06p08331>

490 Comiso, J. C., Kwok, R., Martin, S., & Gordon, A. L. (2011). Variability and trends in sea ice
491 extent and ice production in the Ross Sea. *Journal of Geophysical Research*, 116(C4)
492 <http://doi.org/10.1029/2010JC006391>

493 Egbert, G. D., & Erofeeva, S. Y. (2002). Efficient Inverse Modeling of Barotropic Ocean Tides.
494 *JOURNAL OF ATMOSPHERIC AND OCEANIC TECHNOLOGY*, 19(2), 183-204.
495 [http://doi.org/10.1175/1520-0426\(2002\)019<0183:EIMOBO>2.0.CO;2](http://doi.org/10.1175/1520-0426(2002)019<0183:EIMOBO>2.0.CO;2)

496 Gordon, A. L., & Huber, B. A. (1990). Southern ocean winter mixed layer. *Journal of
497 Geophysical Research*, 95, 11655-11672.

498 Hannah, C. G., Dupont, F., & Dunphy, M. (2009). Polynyas and Tidal Currents in the Canadian
499 Arctic Archipelago. *ARCTIC*, 62(1), 83-95. <http://doi.org/10.14430/arctic115>

500 Hausmann, U., Sallée, J. B., Jourdain, N. C., Mathiot, P., Rousset, C., Madec, G., Deshayes, J.,
501 & Hattermann, T. (2020). The Role of Tides in Ocean - Ice Shelf Interactions in the
502 Southwestern Weddell Sea. *Journal of Geophysical Research: Oceans*, 125(6)
503 <http://doi.org/10.1029/2019JC015847>

504 Hellmer, H. H., Kauker, F., Timmermann, R., Determann, J., & Rae, J. (2012). Twenty-first-

- 505 century warming of a large Antarctic ice-shelf cavity by a redirected coastal current.
506 *NATURE*, 485(7397), 225-228. <http://doi.org/10.1038/nature11064>
- 507 Hogan, K. A., Larter, R. D., Graham, A. G. C., Arthern, R., Kirkham, J. D., Totten Minzoni, R.,
508 Jordan, T. A., Clark, R., Fitzgerald, V., Wåhlin, A. K., Anderson, J. B., Hillenbrand, C.,
509 Nitsche, F. O., Simkins, L., Smith, J. A., Gohl, K., Arndt, J. E., Hong, J., & Wellner, J.
510 (2020). Revealing the former bed of Thwaites Glacier using sea-floor bathymetry:
511 implications for warm-water routing and bed controls on ice flow and buttressing. *The*
512 *Cryosphere*, 14(9), 2883-2908. <http://doi.org/10.5194/tc-14-2883-2020>
- 513 Huot, P., Fichet, T., Jourdain, N. C., Mathiot, P., Rousset, C., Kittel, C., & Fettweis, X. (2021).
514 Influence of ocean tides and ice shelves on ocean – ice interactions and dense shelf water
515 formation in the D ’ Urville Sea, Antarctica. *OCEAN MODELLING*, 162, 101794.
516 <http://doi.org/10.1016/j.ocemod.2021.101794>
- 517 Jacobs, S., Jenkins, A., Hellmer, H., Giulivi, C., Nitsche, F., Huber, B., & Guerrero, R. (2012).
518 The Amundsen Sea and the Antarctic Ice Sheet. *OCEANOGRAPHY*, 25(3), 154-163.
519 <http://doi.org/> <http://dx.doi.org/10.5670/oceanog.2012.90>
- 520 Jourdain, N. C., Molines, J., Le Sommer, J., Mathiot, P., Chanut, J., de Lavergne, C., & Madec,
521 G. (2019). Simulating or prescribing the influence of tides on the Amundsen Sea ice shelves.
522 *OCEAN MODELLING*, 133, 44-55.
523 <http://doi.org/https://doi.org/10.1016/j.ocemod.2018.11.001>
- 524 Kim, S., Lim, D., Rebolledo, L., Park, T., Esper, O., Muñoz, P., La, H. S., Kim, T. W., & Lee, S.
525 (2021). A 350-year multiproxy record of climate-driven environmental shifts in the
526 Amundsen Sea Polynya, Antarctica. *GLOBAL AND PLANETARY CHANGE*, 205, 103589.
527 <http://doi.org/10.1016/j.gloplacha.2021.103589>

- 528 Lee, Y. C., Park, M. O., Jung, J., Yang, E. J., & Lee, S. H. (2016). Taxonomic variability of
529 phytoplankton and relationship with production of CDOM in the polynya of the Amundsen
530 Sea, Antarctica. *Deep Sea Research Part II: Topical Studies in Oceanography*, 123, 30-41.
531 <http://doi.org/10.1016/j.dsr2.2015.09.002>
- 532 Macdonald, G. J., Ackley, S. F., & Mestas-Nuñez, A. M. (2021). Evolution of the Amundsen Sea
533 Polynya, Antarctica, 2016-2021. *The Cryosphere Discussions*(2021), 1-33.
534 <http://doi.org/10.5194/tc-2021-250>
- 535 Markus, T., & Burns, B. A. (1993). Detection of coastal polynyas with passive microwave data.
536 *ANNALS OF GLACIOLOGY*, 17, 351-355.
- 537 Martin, S. (2004). Okhotsk Sea Kashevarov Bank polynya: Its dependence on diurnal and
538 fortnightly tides and its initial formation. *Journal of Geophysical Research*, 109(C9)
539 <http://doi.org/10.1029/2003JC002215>
- 540 Massom, R. A., Harris, P. T., Michael, K. J., & Potter, M. J. (1998). The distribution and
541 formative processes of latent-heat polynyas in East Antarctica. In W. F. Budd (Ed.),
542 *ANNALS OF GLACIOLOGY* (27, pp. 420-426). (Reprinted.
- 543 Meehl, G. A., Arblaster, J. M., Chung, C. T. Y., Holland, M. M., DuVivier, A., Thompson, L.,
544 Yang, D., & Bitz, C. M. (2019). Sustained ocean changes contributed to sudden Antarctic
545 sea ice retreat in late 2016. *Nature Communications*, 10(1) [http://doi.org/10.1038/s41467-](http://doi.org/10.1038/s41467-018-07865-9)
546 [018-07865-9](http://doi.org/10.1038/s41467-018-07865-9)
- 547 Melling, H., Lake, R. A., Topham, D. R., & Fissel, D. B. (1984). Oceanic thermal structure in the
548 western Canadian Arctic. *CONTINENTAL SHELF RESEARCH*, 3(3)
- 549 Morales Maqueda, M. A., Willmott, A. J., & Biggs, N. R. T. (2004). Polynya dynamics; a review
550 of observations and modeling. *Reviews of geophysics* (1985), 42(1), G1001-G1004.

551 <http://doi.org/10.1029/2002RG000116>

552 Nakayama, Y., Cilan, C., & Seroussi, H. (2021). Impact of subglacial freshwater discharge on

553 Pine Island ice shelf. *GEOPHYSICAL RESEARCH LETTERS*, 48(18)

554 <http://doi.org/10.1029/2021GL093923>

555 Nitsche, F. O., Jacobs, S. S., Larter, R. D., & Gohl, K. (2007). Bathymetry of the Amundsen Sea

556 continental shelf: Implications for geology, oceanography, and glaciology. *Geochemistry,*

557 *Geophysics, Geosystems*, 8(10), n/a-n/a. <http://doi.org/10.1029/2007GC001694>

558 Ou, H. W. (1991). Some effects of a seamount on oceanic flows. *JOURNAL OF PHYSICAL*

559 *OCEANOGRAPHY*, 21(12), 1835-1845. <http://doi.org/10.1175/1520->

560 [0485\(1991\)021<1835:SEOASO>2.0.CO;2](http://doi.org/10.1175/1520-0485(1991)021<1835:SEOASO>2.0.CO;2)

561 Parkinson, C. L. (1983). On the Development and Cause of the Weddell Polynya in a Sea Ice

562 Simulation. *JOURNAL OF PHYSICAL OCEANOGRAPHY*, 13(3), 501-511.

563 [http://doi.org/10.1175/1520-0485\(1983\)013<0501:OTDACO>2.0.CO;2](http://doi.org/10.1175/1520-0485(1983)013<0501:OTDACO>2.0.CO;2)

564 Penwarden, A. D. (1973). Acceptable wind speeds in towns. *Building Science*, 8(3), 259-267.

565 Preusser, A., Ohshima, K. I., Iwamoto, K., Willmes, S., & Heinemann, G. (2019). Retrieval of

566 Wintertime Sea Ice Production in Arctic Polynyas Using Thermal Infrared and Passive

567 Microwave Remote Sensing Data. *JOURNAL OF GEOPHYSICAL RESEARCH-OCEANS*,

568 124(8), 5503-5528. <http://doi.org/10.1029/2019JC014976>

569 Richter, O., Gwyther, D. E., King, M. A., & Galton-Fenzi, B. K. (2022). The impact of tides on

570 Antarctic ice shelf melting. *The Cryosphere*, 16(4), 1409-1429. <http://doi.org/10.5194/tc-16->

571 [1409-2022](http://doi.org/10.5194/tc-16-1409-2022)

572 Rignot, E., Mouginot, J., Scheuchl, B., van den Broeke, M., van Wessem, M. J., & Morlighem,

573 M. (2019). Four decades of Antarctic Ice Sheet mass balance from 1979 - 2017.

- 574 *Proceedings of the National Academy of Sciences*, 116(4), 1095-1103.
575 <http://doi.org/10.1073/pnas.1812883116>
- 576 Rippeth, T. P., Lincoln, B. J., Lenn, Y., Green, J. A. M., Sundfjord, A., & Bacon, S. (2015).
577 Tide-mediated warming of Arctic halocline by Atlantic heat fluxes over rough topography.
578 *Nature Geoscience*, 8(3), 191-194. <http://doi.org/10.1038/ngeo2350>
- 579 Schlosser, E., Haumann, F. A., & Raphael, M. N. (2018). Atmospheric influences on the
580 anomalous 2016 Antarctic sea ice decay. *The Cryosphere*, 12(3), 1103-1119.
581 <http://doi.org/10.5194/tc-12-1103-2018>
- 582 Shepherd, A., Gilbert, L., Muir, A. S., Konrad, H., McMillan, M., Slater, T., Briggs, K. H.,
583 Sundal, A. V., Hogg, A. E., & Engdahl, M. E. (2019). Trends in Antarctic Ice Sheet
584 Elevation and Mass. *GEOPHYSICAL RESEARCH LETTERS*, 46(14), 8174-8183.
585 <http://doi.org/10.1029/2019GL082182>
- 586 Shepherd, A., & Wingham, D. (2007). Recent sea-level contributions of the Antarctic and
587 Greenland ice sheets [Journal Article]. *SCIENCE*, 315(5818), 1529-1532.
588 <http://doi.org/10.1126/science.1136776>
- 589 Spence, P., Holmes, R. M., Hogg, A. M., Griffies, S. M., Stewart, K. D., & England, M. H.
590 (2017). Localized rapid warming of West Antarctic subsurface waters by remote winds.
591 *Nature Climate Change*, 7(8), 595-603. <http://doi.org/10.1038/nclimate3335>
- 592 Spreen, G., Kaleschke, L., & Heygster, G. (2008). Sea ice remote sensing using AMSR-E 89-
593 GHz channels. *Journal of Geophysical Research*, 113(C2)
594 <http://doi.org/10.1029/2005JC003384>
- 595 Stammerjohn, S., Massom, R., Rind, D., & Martinson, D. (2012). Regions of rapid sea ice
596 change: An inter-hemispheric seasonal comparison. *GEOPHYSICAL RESEARCH*

- 597 *LETTERS*, 39(6), n/a-n/a. <http://doi.org/10.1029/2012GL050874>
- 598 Thompson, T. (2022). Antarctic sea ice hits lowest minimum on record. *NATURE*
599 <http://doi.org/10.1038/d41586-022-00550-4>
- 600 Thuróczy, C., Alderkamp, A., Laan, P., Gerringa, L. J. A., Mills, M. M., Van Dijken, G. L., De
601 Baar, H. J. W., & Arrigo, K. R. (2012). Key role of organic complexation of iron in
602 sustaining phytoplankton blooms in the Pine Island and Amundsen Polynyas (Southern
603 Ocean). *Deep Sea Research Part II: Topical Studies in Oceanography*, 71-76, 49-60.
604 <http://doi.org/10.1016/j.dsr2.2012.03.009>
- 605 Tozer, B., Sandwell, D. T., Smith, W. H. F., Olson, C., Beale, J. R., & Wessel, P. (2019). Global
606 Bathymetry and Topography at 15 Arc Sec: SRTM15+. *Earth and Space Science*, 6(10),
607 1847-1864. <http://doi.org/10.1029/2019EA000658>
- 608 Vincent, R. F., & Marsden, R. F. (2008). A Study of Tidal Influences in the North Water
609 Polynya Using Short Time Span Satellite Imagery. *ARCTIC*, 61(4), 373-380.
610 <http://doi.org/10.14430/arctic45>
- 611 Wessel, P., Luis, J. F., Uieda, L., Scharroo, R., Wobbe, F., Smith, W. H. F., & Tian, D. (2019).
612 The Generic Mapping Tools Version 6. *Geochemistry, Geophysics, Geosystems*, 20(11),
613 5556-5564. <http://doi.org/10.1029/2019GC008515>
- 614 Zhang, Y., Zhang, Y., Xu, D., Chen, C., Shen, X., Hu, S., Chang, L., Zhou, X., & Feng, G.
615 (2021). Impacts of atmospheric and oceanic factors on monthly and interannual variations of
616 polynya in the East Siberian Sea and Chukchi Sea. *Advances in Climate Change Research*,
617 12(4), 527-538. <http://doi.org/10.1016/j.accre.2021.07.005>